Lifetime Measurements of the Collision-Free Slow Fluorescence from Glyoxal S_1/T_1 Gateway Levels in a Beam

Ch. Görling, E. Jalviste,† N. Ohta,‡ and Ch. Ottinger*

Max-Planck-Institut für Strömungsforschung, Bunsenstrasse 10, D-37073 Göttingen Germany

Received: August 25, 1998; In Final Form: October 23, 1998

Rotationally cold (40 K) glyoxal molecules were prepared by seeding in a pulsed argon jet and were excited in the 0_0^0 band of the $S_1 \leftarrow S_0$ transition by a pulsed dye laser. Using an intracavity etalon, the resolution was improved compared to previous work from this laboratory. A total of 23 long-lived S_1/T_1 gateway levels were identified by means of their slow (30−80 μs) fluorescence, including 10 found in the earlier study. For eight of them, time-resolved measurements of the fluorescence decay were made. In the range 40−120 μs, they yielded well-defined, single exponentials, indicating that each S_1 gateway level couples with only one T_1 level. Lifetimes between $\tau = 23$ and 83 μs were measured. In some cases a lengthening of τ by up to 50% with increasing laser intensity was observed. It is ascribed to additional S_1/S_0 coupling within the power-broadened absorption line. Two gateway levels exhibited quantum beats at 76 and 64 kHz, respectively. The mechanism producing such slow beats within the small-molecule, two-state S_1/T_1 coupling is not yet understood.

I. Introduction

The singlet−triplet coupling is a fundamental problem in the photochemistry of organic molecules. A much studied example is the case of glyoxal. It has several favorable spectroscopic properties that make this molecule especially well suited for studies of singlet−triplet intersystem crossing (ISC) effects.[1−5] (i) The $S_1 \leftarrow S_0$ electronic transition lies in the visible region and exhibits a highly structured spectrum.[1] (ii) The good $S_1 \rightarrow S_0$ fluorescence quantum yield facilitates methods that rely on fluorescence detection. (iii) The vibrational and most of the rotational structure of the vibronic bands of glyoxal can be resolved with standard pulsed dye lasers.[3] (iv) Owing to the nπ* character of the glyoxal S_1 and T_1 states, the oscillator strength of the spin-forbidden $T_1 \leftarrow S_0$ transition is only about 10^3 times smaller than that of the $S_1 \leftarrow S_0$ excitation;[4] this makes it feasible to detect laser-induced phosphorescence under jet conditions.[5] (v) Near the S_1 origin, the T_1 vibrational level density is low, since there are only 12 normal modes in this molecule, and the S_1-T_1 separation is unusually small (2776 cm^{-1} [6]). Consequently, the S_1/T_1 interaction of glyoxal can be described in terms of the so-called "small-molecule limit".[7−9] However, it will be shown in this work that this is not synonymous with the "weak-coupling model", contrary to what is often assumed.

In the standard nondegenerate two-level coupling scheme, a pair of zero order singlet and triplet states at the close-lying energies $E_s^{(0)}$ and $E_t^{(0)}$ form two eigenstates with energies E_s and E_t

$$E_s = E_s^{(0)} \pm \sqrt{(\Delta E^{(0)}/2)^2 + V^2}$$
$$E_t = E_t^{(0)} \mp \sqrt{(\Delta E^{(0)}/2)^2 + V^2} \tag{1}$$

where V is the S_1/T_1 coupling matrix element and $\Delta E^{(0)} = E_s^{(0)} - E_t^{(0)}$. The corresponding eigenvectors $|s\rangle$ and $|t\rangle$ are mixtures of zero order wave functions $|s^{(0)}\rangle$ and $|t^{(0)}\rangle$

$$|s\rangle = \alpha|s^{(0)}\rangle + \beta|t^{(0)}\rangle$$
$$|t\rangle = -\beta|s^{(0)}\rangle + \alpha|t^{(0)}\rangle \tag{2}$$

where the mixing coefficients α and β obey the normalization condition $\alpha^2 + \beta^2 = 1$. They are therefore usually expressed in terms of a so-called mixing angle θ as

$$\alpha = \cos(\theta/2)$$
$$\beta = \sin(\theta/2) \tag{3}$$

θ is related to the energy difference of the zero order levels, $\Delta E^{(0)}$, and to the energy difference of the eigenstates $\Delta E = E_s - E_t$ by the relations

$$\tan\theta = 2V/\Delta E^{(0)}$$
$$\sin\theta = 2V/\Delta E \tag{4}$$

For unperturbed rotational levels in the vibrational ground states of S_1 and T_1 glyoxal, lifetimes $\tau_s^{(0)} = 2.41$ μs[3] and $\tau_t^{(0)} = 3.29$ ms[10] have been measured. The lifetimes τ_s and τ_t of the states $|s\rangle$ and $|t\rangle$ fulfill the conditions[11]

$$1/\tau_s = \alpha^2/\tau_s^{(0)} + \beta^2/\tau_t^{(0)} \tag{5a}$$

$$1/\tau_t = \beta^2/\tau_s^{(0)} + \alpha^2/\tau_t^{(0)} \tag{5b}$$

The coefficients α and β are conventionally chosen such that $\alpha > \beta$ (and usually $\alpha \gg \beta$). Thus the eigenstate labeled by $|s\rangle$ has mainly singlet character, and $|t\rangle$ has mainly triplet character. From (5a) then follows, to a very good approximation,

$$\tau_s = \tau_s^{(0)}/\alpha^2 \tag{6a}$$

As long as β^2 is not too small, (5b) can also be simplified and

* Corresponding author. Fax: ++49-551-5176-607.
† Permanent address: Institute of Physics, Tartu University, Riia 142, 51014 Tartu, Estonia.
‡ Permanent address: Department of Molecular Chemistry, Graduate School of Engineering, Hokkaido University, Sapporo 060-8628, Japan.

10.1021/jp983518m CCC: $15.00
Published on Web 12/05/1998

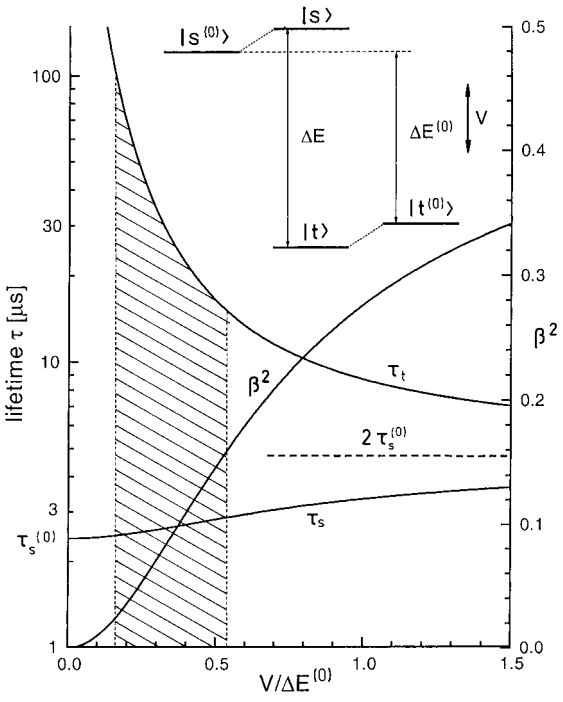

Figure 1. Lifetimes τ_t and τ_s of the perturbed states and the mixing coefficient β^2, as a function of the ratio of coupling strength V and energy spacing $\Delta E^{(0)}$ of the unperturbed levels in a two-level coupling model. In the limit $V \gg \Delta E^{(0)}$, τ_t and τ_s approach the value $2\tau_s^{(0)} = 4.82$ μs (dashed line), at $\beta^2 = 0.5$. The hatched area is delimited by the mean lifetimes τ_t of the slow fluorescence, which are accessible in the present experiment (from 15 μs to 100 μs). The relative energy level spacings in the inset correspond to $V/\Delta E^{(0)} = 0.4$, $\beta^2 = 0.108$, $\tau_t = 22$ μs.

gives

$$\tau_t = \tau_s^{(0)}/\beta^2 \tag{6b}$$

This approximation holds to within 2% or better for the range of β^2 values measured in this work ($\beta^2 \geq 0.03$, see below). The slow fluorescence observed in the present study is emitted by the eigenstate $|t\rangle$ and, from (6), has a lifetime $\tau_t > \tau_s > \tau_s^{(0)}$. $|t\rangle$ and $|s\rangle$ are also called "gateway" states since they connect the singlet and triplet manifolds. This term is illustrated especially nicely in the present experiment, since here the nominal "triplet" state $|t\rangle$ is optically excited via its singlet component $\beta|s^{(0)}\rangle$, and likewise it is this singlet component through which the subsequent slow fluorescence of $|t\rangle$ occurs.

Figure 1 presents the calculated lifetimes τ_s and τ_t and the coefficient β^2, plotted as functions of the ratio $V/\Delta E^{(0)}$. All measurements of this work refer to the branch labeled "τ_t". The shaded area shows the range of parameters that apply to this experiment.

The terms "slow fluorescence" and "prompt fluorescence" are adopted here from the work of Michel and Tramer,[8] where the existence of long-lived fluorescence was theoretically predicted for glyoxal. In the lifetime measurements of ref 8, however, only the prompt component could be detected (corresponding to the branch labeled "τ_s" in Figure 1). We note that the slow fluorescence might also be called fast phosphorescence, emphasizing the dominant triplet character of the emitting gateway state. The term prompt fluorescence denotes in our article the emission from the singlet-like eigenstate $|s\rangle$ of the coupled S_1/T_1 pairs under study (having, from Figure 1, lifetimes between ~2.5 and ~2.8 μs), as well as the fluorescence from uncoupled levels of S_1 (with lifetime $\tau_s^{(0)} = 2.41$ μs).

It should be noted that the terms fast (or prompt) and slow fluorescence decay have been used in the literature with a different meaning (e.g., see refs 11 and 12). In the context of discussing so-called intermediate-coupling case molecules, where a large number of triplet states are involved with mixing coefficients of comparable size, the terms "fast" and "slow" denote, respectively, the dephasing and the population decay of a coherently prepared superposition state. This is a physical situation quite different from the two-state coupling pertaining to the present work.

Although in the past the experimental search for slow fluorescence (in our meaning) of glyoxal was unsuccessful,[8] a few gateway states were identified by enhanced phosphorescence in a low-pressure cell experiment.[9] First convincing experimental observation of slow fluorescence of glyoxal cooled in a free jet was reported from this laboratory by Heldt et al.[13] under carefully established collision-free conditions. The slow fluorescence signal was collected in a time interval from 30 to 80 μs after the laser pulse. Scanning the laser yielded slow fluorescence excitation spectra. Compared to the usual laser-induced fluorescence excitation spectra, they were quite sparse. The analysis showed that they consisted of a selection from the ensemble of lines that make up the full, rather dense prompt fluorescence excitation spectra. Only those few excited levels that have just the right strength of S_1/T_1 coupling to produce lifetimes within the experimental observation window contribute to the slow fluorescence. From a simulation of the $S_1 \leftarrow S_0$ spectrum, in ref 13 the rotational quantum numbers were determined for 10 gateway states of the 0_0^0 band and for 6 gateway states of the 5_0^1 band. Slow fluorescence was also observed from many other vibrational states of S_1 glyoxal, but no detailed assignment of the gateway levels was made.

The present experiment is a significant extension of the study of Heldt et al.,[13] as regards the 0_0^0 band. With improved spectral resolution, the slow fluorescence excitation spectrum of this band was reinvestigated, and 13 further gateway levels were found, in addition to the 10 previously observed. More importantly, the former work demonstrated only the *existence* of gateway levels with very long lifetimes. Here we present quantitative time-resolved measurements of the slow fluorescence decay from 8 of the gateway levels in the vibrationless S_1 state. The decay was found to be purely exponential, confirming the two-state coupling model, and the "small-molecule" character of glyoxal in this region.

2. Experimental Section

Glyoxal was produced by heating a 1:3 volume mixture of glyoxal trimer dihydrate and P_2O_5 (both from Aldrich) and condensing the released vapor in a liquid nitrogen trap.[13,14] Every 5−10 min the distillation was interrupted to pump off the noncondensable gases. During the experiments, the glyoxal sample was kept at −10 °C in a thermoelectrically cooled housing (Products for Research, type TE 104). After overnight storage at this temperature, impurity gases had to be pumped off again before starting a new experiment. For the measurements, Ar carrier gas at a pressure of ~110 mbar was allowed to flow through the reservoir containing the cooled glyoxal at a vapor pressure of ~10 mbar. The Ar/glyoxal mixture was expanded into vacuum through a General Valve Series 9 pulsed nozzle with an orifice of 0.8 mm diameter. The front of the nozzle housing was blackened to reduce scattered light. The duration of the Ar gas pulse, measured with a fast ionization gauge, was typically 150 μs with a nozzle control pulse 240 μs long. The pulse repetition rate was typically 30 Hz. With two

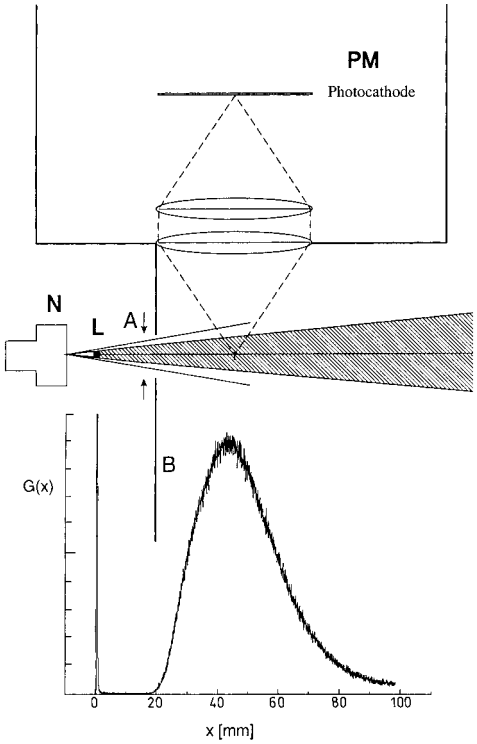

Figure 2. Experimental arrangement (to scale). The pulsed jet issuing from the nozzle N is crossed 10 mm downstream by the laser beam L. The hatched area indicates the volume filled by the excited molecules. Two $f = 40$ mm quartz lenses, centered 44 mm downstream from the excitation region, collect the slow emission from the beam onto the cathode (46 mm diameter) of the photomultiplier (PM). A light baffle (B) with a 15 mm aperture (A) shields the detector from the strong prompt fluorescence. At the bottom, the detection efficiency $G(x)$ is shown as a function of the coordinate x along the jet axis. The shape of $G(x)$ was obtained from time-resolved measurements of the glyoxal phosphorescence (see text). The width of $G(x)$, combined with the beam velocity, determines the range of the experimentally accessible emission lifetimes.

Edwards Diffstak diffusion pumps of 1700 L/s each, the vacuum was 4×10^{-5} Torr during the experiments.

A FL 3002 dye laser, pumped by an EMG 202 MSC excimer laser (both from Lambda Physik), was used to optically excite the glyoxal molecules. The cross section of the unfocused laser beam in the excitation region was about 2×3 mm^2. Unlike the previous work of this group[13] all measurements were performed with the commercially available etalon installed in the dye laser cavity. Coumarin 2 dye was used for the wavelength region of the $S_1 \leftarrow S_0$ origin band near 455 nm and Coumarin 307 dye for the $T_1 \leftarrow S_0$ origin band near 521 nm.

The central part of the arrangement for the measurements of the slow fluorescence is outlined in Figure 2. The laser beam (perpendicular to the plane of the figure) crosses the glyoxal molecular beam 10 mm downstream from the nozzle. The slow fluorescence light is collected onto the photocathode of an EMI 9829 QGA photomultiplier, which was positioned within the vacuum chamber. The multiplier output pulses were fed to a preamplifier plus discriminator (PAR model SSR 1120), which was also located in the vacuum, close to the multiplier. In the lower part of Figure 2 the detection efficiency is plotted as a function of the position (x) of the emitting long-lived molecules along the jet axis (the response function $G(x)$).

A block diagram of the electronic components is given in Figure 3. The arrangement for measurements of slow fluorescence decay times is shown in the box (a) of Figure 3. In these measurements the laser was tuned to a selected excitation line.

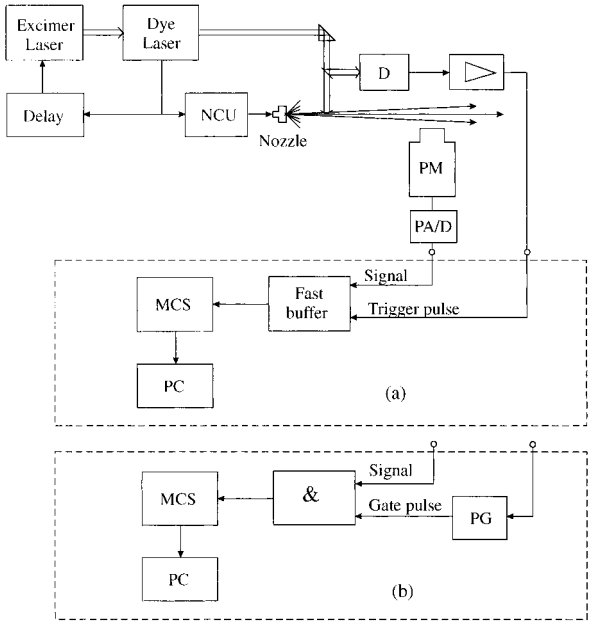

Figure 3. Schematic of the apparatus used for time-resolved measurements (a) and for the measurements of excitation spectra (b). (a) The laser wavelength is kept fixed in this mode. The sequence of time-resolved measurements is controlled by the dye laser clock. It provides trigger pulses for the nozzle control unit (NCU) and also fires the excimer laser with a delay to allow for the nozzle opening time lag. A light signal picked off the laser beam generates a pulse in the photodiode (D). It triggers the fast buffer, causing it to sweep through its 2048 channels with a dwell time of 80 ns per channel. During this sweep the counts from the photomultiplier (PM) and the preamplifier/discriminator (PA/D) are stored in the buffer channels according to their respective arrival time, with a maximum rate of one count per channel per sweep. At the end of the sweep the buffer contents are transferred to the multichannel scaler (MCS). Data from each laser shot are summed in the MCS and are finally processed in the computer (PC). (b) The laser is operated in the "burst" mode (10 shots at each wavelength, which is sequentially incremented, typically by $\Delta\lambda = 44 \times 10^{-6}$ nm). The signals from the PM are admitted to the MCS via an AND gate. The gate is open during a time interval from t_1 to t_2 after each laser pulse, as determined by the photodiode signal and the pulse generator PG. t_1 and t_2 are chosen so as to select prompt fluorescence (PF) or slow fluorescence (SF) signals; see text. Output pulses from the AND gate are stored in one of the MCS channels, until a pulse from an internal clock causes the next MCS channel to be addressed. The rate of channel advance pulses is 1 s^{-1}. After the desired wavelength range has been covered, the accumulated spectrum is read out from the MCS by the PC. The MCS channel advance pulses were not synchronized with the wavelength increments of the dye laser etalon. This resulted in a slight wavelength scale nonlinearity of the spectra ($\sim$0.1 cm^{-1}, comparable to the spectral resolution, across the $\sim$10 cm^{-1} width of each etalon scan).

The slow fluorescence photon counts are distributed between the channels of a fast multichannel analyzer (fast buffer model CMTE-FAST 7885) according to their arrival time after the laser pulse. Finally, the results are processed with a multichannel data acquisition system (multichannel scaler model CMTE-FAST MCD/PC). Depending on the intensity of the signal, data accumulation times ranging from 60 s up to 1800 s were used. For measurements of excitation spectra of either the prompt or the slow fluorescence, a gated photon counting technique was used, as shown in (b). The counts passing the preset time gate were stored and processed as in (a). For slow fluorescence (SF) detection, the gate was set to be open from $t_1 = 30$ μs to $t_2 = 80$ μs after the laser pulse. This discriminates completely against any scattered light from prompt fluorescence (PF). PF excitation spectra, on the other hand, were recorded with a gate interval from 2 to 10 μs. Unlike the previous study,[13] the photomultiplier

was here kept in the downstream position shown in Figure 2 even for PF detection. It was found that a sufficient portion of the very bright prompt fluorescence light reached the detector, despite the light baffle B (Figure 2).

The lifetimes of the gateway states were determined in a manner similar to that described in ref 15. The measured time-dependent signal following the laser excitation pulse is given by

$$I(t) = I_0 \exp\left(-\frac{t}{\tau_t}\right) G(t) \qquad (7)$$

Here τ_t is the slow fluorescence lifetime, and $G(t)$ describes the temporal response function of the detection system. It takes into account all instrumental factors that determine the recorded waveform, with the sole exception of the radiative lifetime. Thus $G(t)$ includes the effects of spatial variation of the detection efficiency over the entire observation volume of the multiplier; the beam velocity distribution; the density distribution of laser-excited molecules across the beam; and the laser pulse width. Fortunately, $G(t)$ can be directly measured as the time-dependent laser-induced phosphorescence (LIP) signal $I_{ph}(t)$. Because of the very long lifetime $\tau_t^{(0)} = 3.3$ ms of the phosphorescence,[10] the exponential in eq 7 is nearly a constant for the time interval of interest ($<150\ \mu$s), and $I_{ph}(t) \propto G(t)$. Division of the measured slow fluorescence signal $I(t)$ by the response function $I_{ph}(t)$ results therefore in an exponential decay curve, which yields the slow fluorescence lifetime. For the LIP measurements the laser was tuned onto an intense feature of the 0_0^0 band of the $T_1 \leftarrow S_0$ transition ($\lambda \sim 520.7$ nm).

The LIP signal expressed as a function of the coordinate $G(x=vt)$ along the jet axis is presented in Figure 2 to emphasize its relationship with the geometry of the light collection optics. The coordinate and time scales are related by the velocity of the Ar carrier gas, which was calculated, for adiabatic expansion, to be $v \sim 0.55$ mm/μs. Note, however, that v need not be known in the present experiment, as long as the velocity distribution is the same for the slow fluorescence and the phosphorescence measurements. Care must therefore be taken to ensure the same jet conditions for these two experiments. This includes the alignment of the jet axis. Even a slight change in geometry between the two measurements resulted in a distorted (nonexponential) decay curve.

3. Results and Discussion

3.1. Slow and Prompt Fluorescence Excitation Spectra. This section describes the reinvestigation of the slow fluorescence excitation spectrum and the assignment of the lines. Compared with the previous measurements,[13] using the intracavity etalon improved the spectral resolution by a factor of about 1.7. A narrow laser bandwidth is vital for the lifetime measurements on isolated excited-state levels; see section 3.2. Also, the nozzle−laser distance d was smaller in the present work ($d = 10$ mm instead of 27 mm), which increased the signal-to-noise ratio while still maintaining collision-free conditions. This is discussed in the Appendix.

Slow fluorescence (SF) and prompt fluorescence (PF) excitation spectra were measured in the region around the $S_1 \leftarrow S_0$ origin located at 21 973.439 cm^{-1}.[16] Partial results, from single etalon scans, are shown in Figure 4. The fwhm resolution is $\sim$0.1 cm^{-1} for the PF and $\sim$0.07 cm^{-1} for the SF spectrum, limited by Doppler broadening. For the PF the full divergence of the molecular beam in the direction of the laser beam is effective, while for the SF spectrum the aperture A (Figure 2) narrows the relevant part of the beam somewhat. The bandwidth of the laser ($\leq$0.04 cm^{-1} according to the etalon specifications) makes only a negligible contribution in this work, while in ref 13, without an etalon, the measured overall line width was 0.12 cm^{-1}.

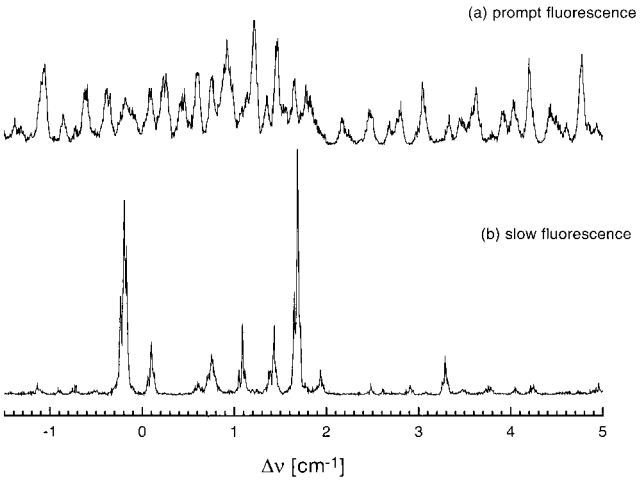

Figure 4. Excitation spectra of the $S_1 \leftarrow S_0$ transition of jet-cooled glyoxal, part of the 0_0^0 band. Top: prompt fluorescence (PF) detection. Bottom: slow fluorescence (SF) detection. The respective time gates were 2−10 and 30−80 μs after the excitation pulse. The PF spectrum was used (a) to identify the lines by rotational quantum numbers, (b) to determine the rotational temperature T_{rot}, and (c) to calibrate the wavelength scale (see text). Comparison with the SF spectrum yields the quantum numbers of the gateway states. Note the much smaller line density in the SF spectrum, reflecting the selectivity of the S_1/T_1 gateways.

A comparison of Figure 4 with the corresponding sections of Figure 3a,b in ref 13 demonstrates clearly the striking effect of the improved resolution, especially in the SF spectra. Of the conspicuous group of three lines in Figure 3a of ref 13, the present Figure 4b shows only the two outer lines, while the central one in ref 13 apparently resulted from several blended smaller components, which are now resolved. For the lifetime measurements described below, sufficient spectral discrimination is very important. In addition, the relative line intensities are different in the present work from those in ref 13 because of slightly different thermal population distributions of the S_0 rotational levels (see below).

PF and SF excitation spectra were taken across the whole width of the $S_1 \leftarrow S_0$ 0_0^0 band, from -22 to $+26$ cm^{-1} relative to the origin frequency. It was covered by five separate overlapping etalon scans, each about 0.22 nm (10 cm^{-1}) wide. Simulations of the PF spectrum (see below) were used as a reference to correct the frequency scale of the individual etalon scans. The corrected five parts of both spectra were then merged. The resulting SF excitation spectrum is presented in the upper half of Figure 5. It is, in principle, equivalent to the spectrum shown in Figure 7b of ref 13. However, owing to the improved resolution of the present work, it exhibits far more lines. The different beam expansion conditions (higher T_{rot}; see below) and a more favorable geometry (shorter nozzle−laser distance) also help to increase the number of detectable SF lines.

As a first step toward the identification of the SF lines, the entire PF excitation spectrum (of which only a section is shown here in Figure 4a) was simulated by computer. It was described as a C-type rigid asymmetric top absorption spectrum. Ground and excited-state rotational constants (including D_J, D_K, and D_{KJ}) were taken from the work of Paldus and Ramsey.[17] The nuclear spin statistical weights, 1 for even K_c states and 3 for odd K_c

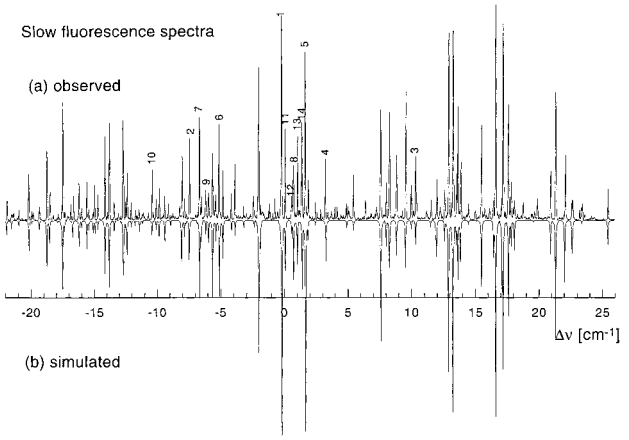

Figure 5. Top: observed slow fluorescence excitation spectrum of the entire 0_0^0 band of the $S_1 \leftarrow S_0$ transition of jet-cooled glyoxal (composite of five wavelength-corrected etalon scans). Bottom: computer simulation, based on a line width of 0.07 cm^{-1} and $T_{rot} = 40$ K. Lines for which the SF lifetime was measured are marked with a number (see Table 2 for their assignments).

states, were properly accounted for. The simulation reproduced the line frequencies of the experimental PF excitation spectrum very well. The observed relative intensities, however, were not completely matched. Overall, the shape of the spectrum was best reproduced by a fit with the rotational temperature of $T_{rot} = 40$ K, significantly different from the value of 15 K obtained in ref 13. This must be due to different nozzle conditions. Some of the discrepancies between the intensity distributions in the calculated 40 K spectrum and the observed spectrum are probably due to experimental reasons. It was found that the relative line intensities of the excitation spectra, for PF as well as SF, were not always reproducible in repeated scans. For example, the relative intensity of the two prominent lines in Figure 4b varied by a factor of 2. This can be explained by uncontrolled changes of the partial pressure of glyoxal and the rotational temperature in the excitation zone. The rotational temperature affects very sensitively the relative intensities of lines originating from high-J and low-J states. For example, raising T_{rot} from 20 to 40 K increases the calculated intensity of the line at -0.19 cm^{-1} relative to that at $+1.67$ cm^{-1} by a factor of 4.8.

Apart from providing the etalon wavelength corrections and establishing a value of T_{rot}, the successful simulation of the PF excitation spectrum forms the basis of the important identification of the gateway states in terms of excited-state rotational quantum numbers J', K_a', K_c'. As in ref 13, this was accomplished by comparing the wavelengths of the observed SF lines with the calculated PF lines. For the latter, the quantum numbers are known from the simulation. However, the PF spectrum is so congested that for any given SF line there are usually several calculated PF lines falling within the width of the SF line in question. The choice among these possible candidates was made in the same way as in ref 13: From the selection rules, any S_1 level combines optically with up to six S_0 levels. Therefore a multiplet of up to six lines in the SF excitation spectrum must be associated with each gateway level. The various calculated transitions $J', K_a', K_c' \leftarrow J'', K_a'', K_c''$ compatible with a given SF line within its line width were considered in turn. For each of these trial assignments, the SF spectrum was searched for the other lines of the multiplet sharing the same upper state J', K_a', K_c'. The trial assignment was only accepted as correct if *all* predicted lines of the multiplet leading into the particular gateway in question were actually observed in the SF excitation spectrum and appeared with the correct

TABLE 1: Rotational Assignments and Slow Fluorescence Intensity Weighting Factors $\bar{\gamma}$ for the Identified S_1/T_1 Gateway States of Glyoxal in the Vibrationless Level of S_1

ref 13[a]	J'	K_a'	K_c' [b]	$\bar{\gamma}$[c]
*	4	1	4	9
	6	4	2 (3)	6 (2)
	7	1	7	0.6
	9	6	3 (4)	1.5 (4.5)
	10	5	5 (6)	1.5 (4.5)
	11	0	11	0.2
*	11	4	7 (8)	7 (21)
*	12	1	12	1.4
	12	3	10	2
*	12	5	7 (8)	6 (12)
*	12	7	5 (6)	5 (15)
	14	0	14	4
*	14	4	10 (11)	21 (7)
*	16	5	11 (12)	5 (15)
*	17	1	17	3
*	17	2	16	4
	17	3	14	2
	19	3	16	5
	19	3	17	3
*	20	1	19	4
	20	4	16 (17)	10 (3.3)
	20	5	15 (16)	5 (15)
	24	1	23	2

[a] The asterisk marks gateway levels already found in ref 13. Their quantum numbers were confirmed in this work. The $\bar{\gamma}$ values cannot be compared with ref 13 due to different experimental conditions. [b] The numbers in parentheses are the alternative assignment for K_c'. [c] $\bar{\gamma}$ is a weighting factor (in arbitrary units) used for calculating the line intensities of the simulated slow fluorescence excitation spectrum from the intensities of the simulated C-type asymmetric top spectrum of glyoxal for $T_{rot} = 40$ K. The same value of $\bar{\gamma}$ is used for the intensities of all lines belonging to a given gateway state J', K_a', K_c'. $\bar{\gamma}$ values in parentheses are for the alternative assignments of K_c' as given in column 4 in parentheses.

intensity pattern (excepting only lines that were clearly blended or were calculated to be very weak; in practice, of each multiplet at least three unambiguous SF lines were found).

With this technique of proposing trial assignments and probing their validity, it was possible to identify 23 gateway levels in the S_1 state. Their rotational quantum numbers are given in Table 1. All 10 earlier assignments[13] were confirmed. The assignment of the 23 gateway levels was based on a total of ~100 individual lines of the SF excitation spectrum in the region from -22 to $+26$ cm^{-1}. These lines are not all listed here; a similar, but smaller listing can be found in Table 1 of ref 13. However, for those 8 gateway levels for which lifetime measurements were made in this work (see section 3.2), Table 2 does specify some of the excitation lines, usually the strongest out of each corresponding multiplet. The ~100 identified lines do not fully exhaust the observed SF spectrum. There are a few minor lines for which no consistent assignment could be found. Some of these may belong to the 7_1^1 hot band.

To demonstrate visually the success of the SF line assignments, the entire SF excitation spectrum was simulated. Following ref 13, where a corresponding procedure is described in detail, the measured intensities I_{exp}^{SF} of the identified SF lines were compared to the intensities I_{calc}^{PF} of the corresponding lines in the simulated PF excitation spectrum. All the inherent factors affecting these two intensities are the same (thermal ground state population, statistical weight, and line strength). In addition, however, I_{exp}^{SF} is critically determined by the weight β^2 of the singlet component in the wave function $|t\rangle$, eq 2. The probability to populate $|t\rangle$ by absorption from the S_0 ground state is proportional to β^2. Furthermore, β^2 controls via

TABLE 2: Slow Fluorescence Lifetimes of Glyoxal Resulting from Excitation on Selected $S_1 \leftarrow S_0$ Lines of the 0_0^0 Band

line[a]	J'	K_a'	K_c'	←	J''	K_a''	K_c''	$\Delta\nu$ (cm^{-1})[b]	τ_t (μs)[c]	$\bar{\tau}_t$ (μs)[d]	β^2 [e]
1*	17	1	17	←	17	0	17[f]	−0.19	28 (4)	30[i]	0.08
2*	17	1	17	←	17	2	15	−7.44	32 (10)		
3	17	2	16	←	16	1	16	10.33	52 (6)	51	0.05
4	17	2	16	←	17	1	16	3.29	49 (7)		
5	4	1	4	←	4	0	4	1.67	33 (7)	38[j]	0.06
6	4	1	4	←	4	2	2	−5.09	40 (15)		
7	4	1	4	←	5	2	4	−6.63	42 (5)		
8*	12	1	12	←	12	0	12[g]	0.74	20 (4)	23	0.1
9*	12	1	12	←	12	2	10	−6.15	24 (3)		
10*	12	1	12	←	13	2	12	−10.07	24 (2)		
11	20	1	19	←	19	2	17	0.10	30 (7)	30	0.08
12	24	1	23	←	23	2	21	0.59	35 (11)	35	0.07
13	14	0	14	←	13	1	12	1.04	43 (15)	43	0.06
14	7	1	7	←	7	0	7[h]	1.42	83 (+50−25)	83	0.03

[a] Exciting $S_1 \leftarrow S_0$ line; for the numbering see Figure 5. An asterisk marks those cases where quantum beats were observed in the fluorescence decay. Lines belonging to the same S_1 gateway level are grouped together. [b] Frequency with respect to the band center. [c] Measured slow fluorescence lifetime and its statistical error. [d] Slow fluorescence lifetime of a given gateway state, averaged over the individual measurements from separate exciting lines of that same state. [e] $\beta^2 = \tau_s^{(0)}/\tau_t$, where $\tau_s^{(0)} = 2.41$ μs. [f] Overlapped with the ~20 times weaker line 17, 2, 16 ← 18, 1, 18 at −0.18 cm^{-1}. [g] Overlapped with the ~7 times weaker line 11, 0, 11 ← 10, 1, 9 at 0.73 cm^{-1}. [h] Overlapped with the ~7 times weaker line 19, 3, 16 ← 20, 2, 18 at 1.39 cm^{-1}. [i] Correction for molecular saturation gives $\tau = 24.5$ μs; cf. Figure 7. [j] Measured with 0.025 laser attenuation to avoid detector saturation, as for the similarly strong line no. 1 (cf. Figure 7). The molecular saturation was also similar for these two lines (see text). It can therefore be approximately accounted for by scaling to the values of line 1. This yields a corrected $\tau = 38 \cdot 24.5/30 = 31$ μs.

eq 6b the probability of emission from $|t\rangle$ occurring within the detection gate interval (30−80 μs, see section 2). β^2 is a priori not known, it varies erratically among the different long-lived levels. The intensity ratio $\gamma = I_{exp}^{SF}/I_{calc}^{PF}$ is therefore an empirical parameter. For the (up to six) lines of a given multiplet, γ should be the same. In ref 13, these γ values were determined separately for each line and averaged over the multiplet. The resulting $\bar{\gamma}$ was then used as an intensity weighting factor of the corresponding multiplet in the simulated SF excitation spectrum. In the present work, for simplicity $\bar{\gamma}$ was treated as a fit parameter. Relative $\bar{\gamma}$ values were assumed for each multiplet, and the simulated intensities of all SF lines were obtained from those of the calculated PF spectrum according to $I_{exp}^{SF} = \bar{\gamma} I_{calc}^{PF}$. The $\bar{\gamma}$ values were then varied, independently for each multiplet, until the simulated composite SF excitation spectrum best matched the observed spectrum. The result is shown in Figure 5, bottom half. The corresponding $\bar{\gamma}$ values are listed in Table 1. As in ref 13, for $K_a' \geq 4$ the K doublets cannot be resolved in this experiment. In this case two alternative K_c' assignments ($K_c' = J' - K_a'$ and $K_c' = J' + 1 - K_a'$) are possible, as given in Table 1, column 4 in parentheses. The intensity weighting factors $\bar{\gamma}$ needed for reproducing the observed intensities in the simulated SF spectrum must then be chosen 3 times larger for the even-K_c' alternative than for the odd K_c', to compensate the effect of nuclear spin statistical weight (which is 3 times larger for odd K_c').

The overall agreement of the observed and the simulated spectrum in Figure 5 is very satisfactory. There are only two exceptions: The SF lines belonging to the $J' = 16$, $K_a' = 5$, $K_c' = 11$ gateway level were found to be about 0.07 cm^{-1} blue-shifted with respect to their calculated position. No other reasonable alternative assignment could be found. Similarly a 0.03 cm^{-1} blue shift was observed for the lines belonging to the $J' = 19$, $K_a' = 3$, $K_c' = 17$ gateway level. The observed shifts imply that these two gateway levels lie at higher energies than predicted. The reason for these slight shifts is at present not understood. However, we note that they are too large to be caused by the S_1/T_1 perturbation. The S_1/T_1 coupling matrix elements for the vibrationless glyoxal are typically in the range from tens up to hundreds of megahertz.[18]

3.2. Slow Fluorescence Lifetimes. This section describes the time-resolved measurements from which the slow fluorescence decay times of some selected gateway levels were determined. The top curve in Figure 6a presents, as an example, the time-resolved signal following the excitation on the line no. 13 (cf. Figure 5a). For the first 20 μs after the laser excitation at $t = 0$, the signal reflects the decay of the prompt fluorescence light penetrating through the aperture A to the PM (see Figure 2). During this time interval the molecules move about 10 mm downstream but are still outside the observation zone of the detector. At $t > 30$ μs the signal is due to the slow fluorescence, which is of central interest in this work. The curve labeled "phosphorescence" shows the apparatus response $G(t)$ to the luminescence from beam particles having essentially infinite radiative lifetime.

Figure 6b shows the true fluorescence decay curve, obtained as the ratio of the "slow fluorescence" and "phosphorescence" curves in (a), cf. eq 7. On the logarithmic intensity scale, the decay curve is linear between 50 and 120 μs. This range is thus selected for fitting the lifetimes of the corresponding purely exponential decay functions. Outside this time interval the data are not reliable. Up to $t \sim 50$ μs the tail of the prompt fluorescence distorts the results (in a two-state model, eq 1, the overall decay is, strictly, always biexponential; see ref 8). At $t > 120$ μs, on the other hand, the signals become too small. We note also that the observation of well-defined exponential decay curves appears to depend critically on operating the laser in the narrow-bandwidth etalon mode.[19] This is ascribed to the improved selectivity in the excitation of isolated long-lived S_1 levels.

Figure 7 presents the decay curves for excitation on line 1, measured with different energies of the laser pulse. It can be seen that the slow fluorescence lifetime increases from 25 to 37 μs with increasing pulse energy. The lifetimes converge to $\tau = 24.5$ μs in the limit of very weak laser pulses. A similar effect was observed by setting the laser to other lines of the SF excitation spectrum, although for weak lines the range of usable pulse energies was smaller. A reliable extrapolation to zero laser power is therefore not always possible.

Figure 7 might suggest that the reason for the apparent increase of the lifetime with increasing laser power is a nonlinearity of the photon counting system at high count rates. This would partly suppress the strongest signals at the top left of the figure and would thus lead to flatter decay curves.

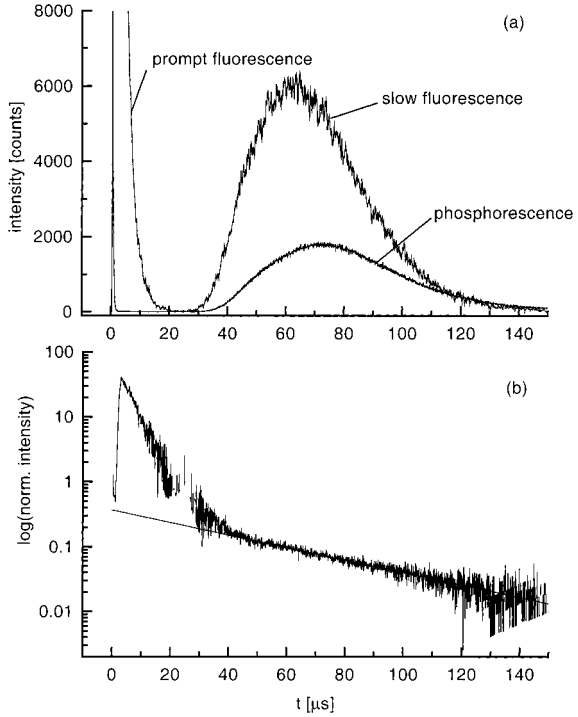

Figure 6. (a) Time-resolved slow fluorescence emission from excitation of the $S_1 \leftarrow S_0$ 0_0^0 band of glyoxal in the blue region (455 nm). The laser was tuned to the J', K_a', $K_c' = 14, 0, 14 \leftarrow J''$, K_a'', $K_c'' = 13, 1, 12$ transition (line no. 13, see Table 2). At $t < 20$ μs stray light of the prompt fluorecence emitted close to the laser beam contributes a fast decaying signal. The signal between 40 and 120 μs is the long-lived fluorescence studied in this work. The curve labeled "phosphorescence" was recorded with the laser tuned to the forbidden $T_1 \leftarrow S_0$ transition in the green region (520.7 nm) and observing the subsequent $T_1 \rightarrow S_0$ laser-induced phosphorescence (LIP) emission. This curve represents the temporal variation of the detection sensitivity (apparatus function) $G(t)$ (cf. Figure 2). The data accumulation time was 600 s for both fluorescence and phosphorescence detection. However, for the former the laser beam was attenuated by a filter of transmission 0.025. (b) Slow fluorescence signal divided by the phosphorescence signal, plotted on a semilogarithmic scale. From a linear fit in the region from 50 to 120 μs the lifetime $\tau_t = 43 \pm 15$ μs is obtained.

However, estimates show that such instrumental effects can be excluded. The multichannel buffer (model FAST 7885) can only accept one count per laser shot and channel. In the example of Figure 7 (line no. 1), with 1800 shots (i.e., for a data accumulation time of 60 s, at the laser repetition rate of 30 Hz) at full laser power, about 400 counts were registered in each channel near the maximum of the signal curve. This corresponds to 0.22 counts per laser shot and channel, well below the limit of the buffer.

Another experimental limit is set by the preamplification/discriminator (PAR, model SSR 1120). It begins to be nonlinear at an average count rate of 1 MHz (at 10 MHz the saturation is complete). In the above example, the average 0.22 counts per buffer channel arrived within the channel width of the FAST module, which was set to 80 ns in this experiment. This corresponds to an average photon rate of 2.7 MHz, which is, in fact, a little above the permissible limit. However, Figure 7 shows that, even with a 10 times attenuated laser beam, the apparent lifetime (30.7 μs) has not yet reached its asymptotic value of ~24.5 μs. It is therefore unlikely that the laser power dependence of the lifetimes is due to instrumental artifacts.

We believe that the lifetime lengthening at high laser pulse energy results from the saturation of the molecular transition itself. In ref 20, saturation of the prompt fluorescence of glyoxal

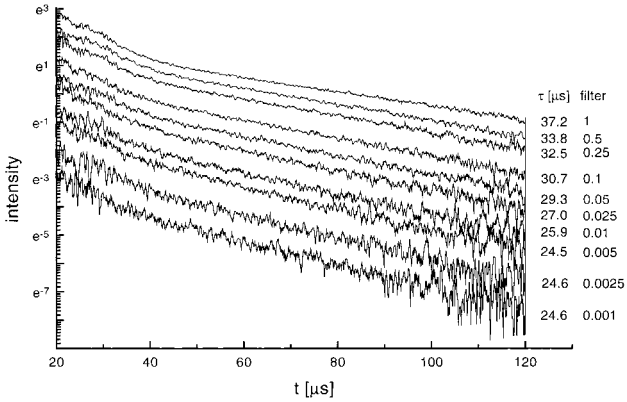

Figure 7. Slow fluorescence decay of the glyoxal S_1/T_1 gateway level excited on line no. 1 (see Table 2), for different laser intensities. The intensity was varied by placing neutral density filters in the laser beam, with calibrated transmission factors as given on the right. The unattenuated laser pulse energy was ~2.5 mJ, and the beam cross section was about 2×3 mm^2. The curves are slightly smoothed. They are normalized to equal data accumulation times, although for the lower curves a 10 times longer signal integration was used. The lifetimes, obtained from fits to the 50−120 μs sections, are given on the right. At high laser intensity, power broadening is believed to induce additional S_1 state couplings and thus lengthen the lifetime (see text). The correct lifetime is obtained by extrapolation to zero laser power (filter transmission <0.01).

has been reported to set in at pulse energies as small as 10 μJ (for the Q branch, $K_a = 0 \leftarrow 1$ excitation of the 0_0^0 band), with an expanded laser beam cross section of 0.25 cm^2. This energy density corresponds in our experiment to that of the most strongly (0.001 filter) attenuated 2.5 mJ pules, across the 0.06 cm^2 beam area. With the lesser attenuation usually employed, our measurements should therefore have been within the saturated regime. It was, in fact, observed that the slow fluorescence intensity I_f did not increase linearly with the laser intensity I_l but followed a power law $I_f \propto I_l^{0.7}$ over the entire attenuation range of 3 orders of magnitude, for lines no. 1 and no. 5. The saturation will be accompanied by power broadening (equivalent to the so-called AC Stark effect) of the molecular transitions (although this was not directly observable in the presence of the dominant Doppler width of ~0.1 cm^{-1}). We suggest that this power broadening causes the observed lifetime lengthening. For sufficiently strong laser pulses the simple two-level singlet−triplet coupling scheme of eq 2 may no longer apply. Additional long-lived states will fall within the power-broadened width of the $S_1 \leftarrow S_0$ transition. The mixture of states thus prepared will then retain its anomalously long lifetime even after the end of the short (~10 ns) laser pulse. One can speculate about the nature of the additional long-lived states. One possibility is the coupling with high-lying levels of the S_0 state, which have a very high density in the vicinity of the S_1 origin. We suggest that under the influence of a strong laser pulse the gateway levels are broadened and couple with a broader range of S_0 levels. An alternative explanation would be an enhanced coupling with the T_1 manifold. However, the vibronic T_1 level density near the S_1 origin is low. It is then unlikely that the broadened gateway levels would encompass additional T_1 levels.

Table 2 summarizes the results of the slow fluorescence lifetime measurements. Data are given for eight gateway levels characterized by J', K'_a, and K'_c (columns 2−4). Altogether, lifetime measurements were made for 14 lines of the $S_1 \leftarrow S_0$ SF excitation spectrum, Figure 5. The first four gateway levels listed in Table 2 were each accessed via two or three different lines. As expected, the individually measured lifetimes τ_t for these different excitation routes are the same within experimental

error. In these cases, as the final result ($\bar{\tau}$) the average of the values τ_t is given.

The observed lifetimes span the range from about 20 to 80 μs. The lower limit of the measurements is set by the interfering contribution of prompt fluorescence; cf. Figure 6. At the other extreme of long lifetimes, the experimental error becomes large, since here the time-resolved slow fluorescence curve differs very little from the mere apparatus response function $G(t)$. In addition, at both ends of the observable range of τ, the intensity factor γ (see above) becomes small. Very short-lived gateways decay too fast to be observed, while too long-lived ones emit too weakly during the transit time through the detection region. The statistical error limits given in Table 2 refer to doubling of the χ^2 fit parameter.

The τ_t values of Table 2 were all obtained using laser beam attenuation filters such that any detector saturation was safely avoided; for example, in the case of line 1 discussed above, attenuation factors of 0.05 and 0.025 were used. Thus stronger lines were investigated with a greater beam attenuation than weaker lines. However, this is not a safeguard against molecular saturation effects, which may well be present even if a line is naturally weak (and was therefore studied at high laser power). The observed intensity of a SF line depends on four factors: (a) the rotational line strength, (b) the degeneracy factor $(2J + 1)$ and the nuclear spin statistical weight, (c) the relative thermal population of the lower level, and (d) the instrumental factor γ, which is a measure of how well the lifetime matches the temporal observation window of the apparatus. If a line is weak because its line strength is small, then molecular saturation is not a problem. If, on the other hand, a line is weak for one of the reasons (b)−(d), then extrapolation to zero laser power would be necessary to obtain the true lifetimes. Since this is not possible for lines that are so weak that they are only detectable at high laser power, the τ values stated in these cases can only be regarded as upper limits. The maximum possible error can be estimated. From Figure 7, the lifetime of line no. 1 is shorter by one-third at low laser power, compared to the result without laser attenuation. Similar, less quantitative measurements on line 5 support this factor. Therefore, for some of the lines listed in Table 2, which were so weak that they had to be studied at full laser power, the lifetime may have to be revised downward by at most one-third. Examples are the lines numbered 8 and 14, which have large line strength factors, comparable to those of lines no. 1 (0.630) and no. 5 (0.508). At the same time lines no. 8 and no. 14 have fairly small γ factors (from Table 1, $\gamma = 1.4$ and 0.6, respectively), which makes them rather weak in the spectrum of Figure 5. The lifetime measurement then required fairly high laser power, with possible saturation effects. The remaining 10 lines of Table 2 have much smaller line strengths (average 0.186), and are therefore less susceptible to molecular saturation.

Note that, for the very limited sample of only 8 gateway levels studied in this work, Table 2 does not indicate any correlation of the lifetime with the rotational quantum numbers J', K_a' or K_c'. This is a result of the quasi-random distribution of the coupling strengths between the S_1 and T_1 levels. Among the multitude of rovibrational T_1 levels in the region of the S_1 origin, it is a matter of chance which rotational levels of the vibrationless S_1 state will find a T_1 level nearby with which they can couple. The triplet character in the excited-state wave function, and hence the lifetime τ_t, will critically depend on how closely spaced the coupled zero-order S_1 and T_1 levels lie. For a small energy gap $\Delta E^{(0)}$ between them, τ_t will be smaller as well (assuming that the coupling constant V is approximately the same; see Figure 1). Thus the irregular distribution of observed lifetimes reflects the random distribution of the $\Delta E^{(0)}$ values. A direct influence of the magnitude of the quantum numbers J', K_a', K_c' on τ_t, if any, could only be detected if $\Delta E^{(0)}$ were known with great precision. However, no such information is at present available.

From Table 2, the coupling parameters measured in this work lie in the range $\beta^2 = 0.03-0.1$ (or $\beta \sim 0.17-0.31$). This can be compared with an estimate given in ref 8. Here, from measurements of the lifetime τ_s, i.e., the short-lived (prompt) fluorescence component, only an upper limit could be obtained, which was $\beta^2 \leq 0.03$. The present, detailed results show that the coupling is actually quite strong, and even exceeds the upper limit deduced in the early work.[8]

According to eqs 3 and 4, we have approximately $\beta = V/\Delta E^{(0)}$ (for not too large values of β). With a coupling matrix element V in the range of 10−360 MHz[18,21] (roughly 3×10^{-4} to 10^{-2} cm^{-1}), the separation of the coupled zero-order singlet and triplet levels spans the range of $\Delta E^{(0)} = 10^{-3}$ to 6×10^{-2} cm^{-1}.

This result supports the validity of the two-state coupling model (2) assumed throughout this paper. If the vibronic level density in the T_1 state is about 1 cm^{-1}, as estimated in ref 8, it is then clear that any given S_1 level can only interact with a single rovibronic T_1 level with quantum numbers fulfilling the selection rules. This is not altered if the fine structure of the T_1 levels is taken into account, since of the three FS components, only one will have the suitable J quantum number and the two neighboring rotational levels, which do have FS components with the same J, are too far away.[6] This is not so with the hyperfine sublevels, which have a splitting of ∼100 MHz,[18,22] comparable with the size of V. Rotational levels with even K_c' have a total nuclear spin $I = 0$, so there is no hfs splitting in this case. Thus for the gateway states with even K_c', a given singlet level is coupled with a single triplet level, forming one coupled pair of eigenstates. For the rotational states with odd K_c', however, three degenerate hyperfine levels of the S_1 state are coupled with corresponding nondegenerate hyperfine levels of the T_1 state (see Figure 2 in ref 9 as an example), forming three coupled pairs. The different energy spacings between corresponding triplet and singlet hyperfine levels give, in general, three different lifetimes for the long-lived component of the coupled pairs. Two situations can then exist: (a) The measured lifetime is the average of the lifetimes of different hyperfine sublevels. (b) Only one or two of the three hyperfine levels have a lifetime falling into the measurable range (from 15 to 100 μs). The observed, purely exponential decays show that either, for (a), the three lifetimes are very similar, or that, for (b), only one of them is measurable.

3.3. Quantum Beats. Some of the slow fluorescence decay curves exhibited striking, well-defined periodic undulations. Such undulations are known as "quantum beats" and occur whenever a set of several closely spaced emitting levels is coherently excited by some short pulse. In the slow fluorescence of the type studied here, this phenomenon has not previously been observed. An example is shown in Figure 8, for excitation of the gateway level $J', K_a', K_c' = 12, 1, 12$, via the line no. 8 (see Table 2). Figure 8a shows the raw data in the range 40−110 μs after the laser pulse (cf. the corresponding section of the "slow fluorescence" curve in Figure 6a for another excitation, without such undulations). In Figure 8b the pure beat signal is presented, with elimination of the effects of the bell-shaped temporal detection efficiency distribution of the apparatus and the usual exponential slow fluorescence decay. To this end, (i) the ratio of the fluorescence signal in Figure 8a and the

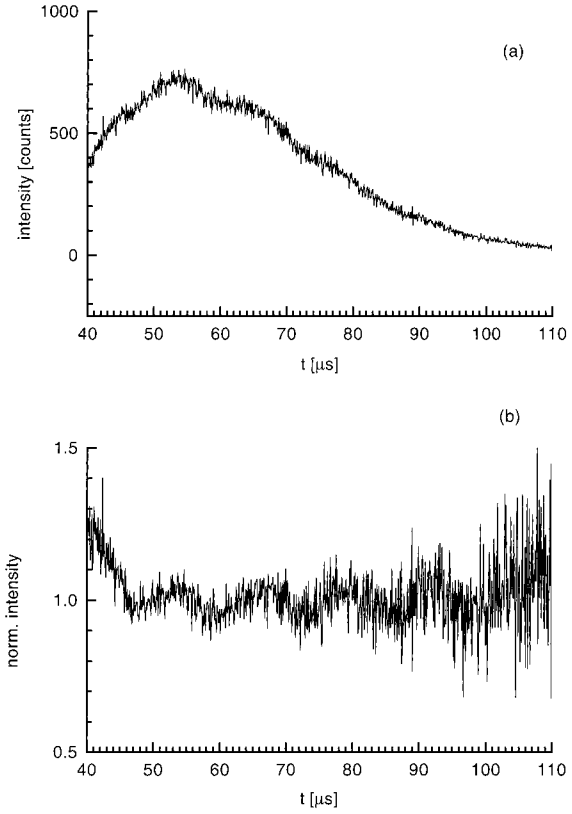

Figure 8. (a) Example of a time-resolved slow fluorescence emission with superimposed quantum beats (excitation on line no. 8, under the usual conditions of 120 mbar nozzle stagnation pressure and a nozzle-laser beam distance of 10 mm). (b) The beat signal, extracted from the raw data in (a) (see text). The beat frequency is ≈76 kHz.

phosphorescence signal $G(t)$ (from Figure 2 or 6a) was plotted semilogarithmically, as in Figure 6b; (ii) a linear decay was then fitted to the 40−110 μs section, also as in Figure 6b; (iii) finally, the slope was eliminated by dividing the result of (i) by that of (ii). The beats now appear as undulations around the value of unity; see Figure 8b. They can be well fitted by a sinusoidal oscillation of 76 kHz. Very similar results were obtained from the excitation of the same gateway level 12, 1, 12 via the line no. 9 or 10 (Table 2). This confirms that the undulations are real and are a characteristic of the upper state of the transition. Quantum beats were also observed on the fluorescence decay from the gateway level 17, 1, 17, and again similarly for both exciting lines, no. 1 and no. 2. In this case the photomultiplier tube was positioned further downstream and covered the time interval from 70 to 150 μs. The dominant beat frequency was here 64 kHz. It is estimated that in the present experiment beat frequencies between 20 and 100 kHz are observable. The contrast of the beat amplitude was smaller for the 17, 1, 17 level than for 12, 1, 12, but increased significantly toward longer times t. Beats of especially high contrast were observed in preliminary experiments on slow fluorescence from glyoxal (S_1) in the vibrationally excited 5^1 level. It should be noted that the quantum beats of the slow fluorescence observed here must be of a different nature from those arising in the *prompt* fluorescence decay through coherent preparation of the states $|s\rangle$ and $|t\rangle$, eq 2.[11] In that case the beat frequency corresponds to the spacing ΔE between $|s\rangle$ and $|t\rangle$ (Figure 1). From (3) and (4), ΔE is of the same order as the coupling matrix element V. In refs 18 and 21, values of V in the range ∼10−360 MHz were measured, with no significant dependence on either the rotational or the vibrational quantum numbers.[21] Beats of 2−6 MHz have, in fact, been observed in the prompt fluorescence of glyoxal.[9] In our experiment, however, the beat frequencies are less than 100 kHz. Such slow beats cannot arise from a pair of states $|s\rangle$ and $|t\rangle$, provided V is as large as given in refs 18 and 21. Moreover, according to eq 7 in ref 11, the amplitude of beats arising from a pair $|s\rangle$, $|t\rangle$ decays with a lifetime close to $2\tau_s^{(0)}$. In glyoxal this would correspond to ∼5 μs. In contrast, the beats reported here were observed in the time span 40−100 μs after the excitation. They are therefore ascribed to a different mechanism, namely the coherent excitation of (at least) *two* triplet-like eigenstates, $|t_1\rangle$ and $|t_2\rangle$, separated by ∼100 kHz, which are both coupled to an S_1 state and are coherently excited. Such a narrow energy gap is consistent with the observation that the appearance of the beats was the same at full laser power and with an attenuated laser beam. Even at vanishing power broadening, the Fourier-limited bandwidth of ∼10 MHz will amply cover both long-lived eigenstates coherently.

Statistically, it is extremely improbable that two independent T_1 levels should lie as close as ∼100 kHz to each other. This would correspond to an average T_1 level density of more than $10^5/\text{cm}^{-1}$, compared to the commonly accepted estimate of $\sim 1/\text{cm}^{-1}$.[8] Thus the hypothetical states $|t_1\rangle$ and $|t_2\rangle$ must be physically related to each other. It is not clear what mechanism could lead to energy splittings as small as this. Hyperfine effects can be excluded. As was mentioned above, the hfs splittings in glyoxal are much larger, on the order of 100 MHz.[18,22] Also the 12, 1, 12 gateway level, with an even-valued K_c', does not have any hfs splitting, yet it shows beats. The most likely explanation, a priori, would appear to be a Zeeman splitting due to stray magnetic fields. In that case, rotating the laser light polarization vector by 90° should change the beat pattern. However, inserting a $\lambda/2$ plate into the laser beam had no effect on the beats.

4. Conclusion

In a small organic molecule such as glyoxal, the important, general problem of S/O coupling between the lowest electronically excited states, S_1 and T_1, can be studied in great detail. This coupling operates only on very specific, isolated S_1 levels, the so-called gateway levels. Through the dominant T_1 character in the wave function, such levels have anomalously long radiative lifetimes. In previous work[13] the first experimental evidence of the predicted "slow fluorescence" from glyoxal gateway levels under collision-free conditions was presented. Several gateway states were identified by their quantum numbers J', K_a', and K_c'. The present work extends this study. Besides adding considerably to the list of identified gateway states, it gives the first quantitative lifetime measurements. For eight gateway levels in the vibrationless trans-glyoxal S_1 state, the fluorescence decay was followed by observing the time-resolved emission from a molecular beam in the range from about 25 to 130 μs after the laser excitation. From the observed single-exponential decays it was concluded that a simple two-state model can describe the coupling situation of these gateways.

Corresponding measurements of vibrationally excited S_1 levels would be of interest, since they would show at what internal energy the two-state coupling breaks down, as a result of the rapidly increasing T_1 level density at higher S_1 excitation energy. Even in the present work, however, in two cases quantum beats were observed to be superimposed on the exponential falloff of the slow fluorescence. Here *two* distinct T_1 levels appear to be coupled to a common S_1 level, giving rise to *two* long-lived, coherently excited eigenstates. The estimated T_1 level density seems far too small to explain this

on the basis of two accidentally coincident gateway couplings. It is much more likely that the two T_1 states in question form an intrinsic pair, split by some very fine interaction, which is at present not yet understood.

Another unexpected observation was that the slow fluorescence lifetime increases significantly with increasing laser power. This may indicate an additional coupling with long-lived states which become accessible within the power-broadened width of the laser-excited gateway level. Highly excited vibrational levels of the electronic ground state, S_0, could be responsible for this effect, since their density is very high in this region.

Acknowledgment. We are grateful for support of this work by the Deutsche Forschungsgemeinschaft (C.G.) and by the Alexander von Humboldt-Stiftung (E.J.). We are also indebted to Dr. B. Sartakov for valuable discussions, to Dr. T. Winkler for much practical advice, and to Mr. G. Shen for his contributions to the experiment.

Appendix: Collisional Effects

In ref 13 it was shown that great care has to be exercised in order to avoid distortion of the slow fluorescence excitation spectrum by collisions. If the gas density in the pulsed jet is too high at the point of laser excitation, then collisional energy transfer from initially excited, short-lived (i.e., nongateway) levels into the long-lived gateway states takes place. This amounts to an admixture of a certain proportion of the prompt fluorescence to the slow fluorescence excitation spectrum (see Figure 3 of ref 13). It was established that positioning the laser excitation region at $d = 27$ mm from the nozzle precluded collisional energy transfer. With $d = 7$ mm, on the other hand, a "slow" spectrum was observed, which was dominated by lines belonging really to the prompt fluorescence excitation.

In those experiments the total stagnation pressure of the nozzle expansion was kept fixed at 105 mbar (13 mbar of glyoxal, plus 92 mbar of Ar), and the gas density at the excitation region was only varied via variation of d. In the present work, the pressure dependence was studied somewhat more systematically, to find the minimum allowed distance d that would still guarantee collision-free excitation, but would at the same time maximize the signal.

Setting $d = 10$ mm, the argon partial pressure was increased from 107 to ~490 mbar; including the glyoxal pressure of 13 mbar, this corresponds to a total stagnation pressure of 120 to ~500 mbar. No significant effect on the slow fluorescence excitation spectrum was seen. Scaled to $d = 7$ mm as used in ref 13, the corresponding pressure range would be ~60−250 mbar, which brackets the value of 105 mbar, where collisional effects were, in fact, clearly observed in ref 13. The reason that this was not the case in the present work is very likely that here the nozzle was mechanically set to produce a much shorter gas pulse than in ref 13, only ~150 μs long compared to 180−200 μs earlier. At very short pulse lengths the nozzle does not open fully; therefore the jet density is smaller at a given stagnation pressure p, and higher values of p can be tolerated. Also related to the short pulse length is probably the less efficient rotational cooling in the present experiment; see section 3.1.

Nevertheless collisional effects could be provoked, using the very short nozzle−laser beam distance of $d = 5$ mm. At 120 mbar, the slow fluorescence excitation spectrum showed first deviations from the truly collision-free spectrum (Figure 4b). At $p = 200$ and 300 mbar, the spectra converged toward the prompt fluorescence spectrum, Figure 4a.

Collisions of the excited molecules manifest themselves not only in the excitation spectrum but also by their effect on the quantum beats. At $p = 200$ mbar the beats were beginning to be distorted, and at higher pressures they were essentially obliterated. The collisional quenching of the beats is caused by relative phase shifts in the wave functions of the coherently excited long-lived states of different molecules. Similar phase shifts are responsible for the well-known collisional line broadening. They occur with a large cross section. This explains why the beat quenching sets in already between 200 and 300 mbar, although the slow fluorescence excitation spectrum did not change significantly up to ~500 mbar. Spectral changes require energy transfer collisions, which have smaller cross sections. In addition they have to occur during the ~2.4 μs lifetime of the excited, nongateway singlet states, while the phase changes of the long-lived, beating states can occur for as long as the molecules are in the region of sufficient density in the jet (~10 μs). For both these reasons the beats are a more sensitive probe for collisional effects than are the spectral changes.

All lifetime measurements reported on in this work were done at $p = 120$ mbar total nozzle stagnation pressure and at a nozzle−laser beam distance $d = 10$ mm. This is well within the region where even the sensitive test based on the beats indicates the absence of collisional effects.

References and Notes

(1) Brand, J. C. D. *Trans. Faraday Soc.* **1954**, *50*, 431.
(2) MacDonald, B. G.; Lee, E. K. C. *J. Chem. Phys.* **1979**, *71*, 5049.
(3) Beyer, R. A.; Zittel, P. F.; Lineberger, W. C. *J. Chem. Phys.* **1975**, *62*, 4016.
(4) McGlynn, S. P.; Azumi, T.; Kinoshita, M. *Molecular Spectroscopy of the triplet state*; Prentice Hall: Englewood Cliffs, NJ, 1969.
(5) Spangler, L. H.; Pratt, D. W. *J. Chem. Phys.* **1986**, *84*, 4789.
(6) Spangler, L. H.; Pratt, D. W.; Birss, F. W. *J. Chem. Phys.* **1986**, *85*, 3229.
(7) Kanamaru, N. *Chem. Phys. Lett.* **1987**, *137*, 487.
(8) Michel, C.; Tramer, A. *Chem. Phys.* **1979**, *42*, 315.
(9) Michel, C.; Lombardi, M.; Jost, R. *Chem. Phys.* **1986**, *109*, 357.
(10) Yardley, J. T. *J. Chem. Phys.* **1972**, *56*, 6192.
(11) N. Ohta, *J. Phys. Chem.* **1996**, *100*, 7289.
(12) van der Werf, R.; Schutten, E.; Kommandeur, J. *Chem. Phys.* **1975**, *11*, 281.
(13) Heldt, J.; Ottinger, Ch.; Vilesov, A. F.; Winkler, T. *J. Phys. Chem. A* **1997**, *101*, 740.
(14) Spangler, L. H.; Matsumoto, Y.; Pratt, D. W. *J. Phys. Chem.* **1983**, *87*, 4781.
(15) Ottinger, Ch.; Vilesov, A. F.; Winkler, T. *Chem. Phys. Lett.* **1993**, *208*, 299.
(16) Birss, F. W.; Brown, J. M.; Cole, A. R. H.; Lofthus, A.; Krishnamachari, S. L. N. G.; Osborne, G. A.; Paldus, J.; Ramsay, D. A.; Watson, L. *Can. J. Phys.* **1970**, *48*, 1230.
(17) Paldus, J.; Ramsay, D. A. *Can. J. Phys.* **1967**, *45*, 1389.
(18) Lombardi, M.; Jost, R.; Michel, C.; Tramer, A. *Chem. Phys.* **1981,** *57***,** 341.
(19) In preliminary experiments without an etalon (Görling, Ch., diploma thesis Göttingen, 1997) the laser had the specified bandwidth of 0.2 cm^{-1}. The lines numbered 1 and 11, which are 0.29 cm^{-1} apart (cf. Table 2) were then not sufficiently resolved, and the overall fluorescence decay was distinctly nonexponential.
(20) Weida, M. J.; Parmenter, C. S. *J. Phys. Chem. A* **1997**, *101*, 9594.
(21) Dupre, P.; Jost, R.; Lombardi, M. *Chem. Phys.* **1984**, *91*, 355.
(22) Katô, H.; Oonishi, T.; Nishizawa, K.; Kasahara, S.; Baba, M. *J. Chem. Phys.* **1997**, *106*, 8392.